Properties of ^{6}Li

Michael E. Gehm

February 25, 2003 (updated 11/2016)

1 Overview

This document is a self contained version of Appendix A of Michael Gehm's Ph.D. Thesis [1]. It attempts to provide many of the important physical properties of bulk and atomic ^{6}Li that are relevant to atomic cooling and trapping experiments. Parameters that result from experimental measurement are referenced to their source (either primary or secondary), while the calculations behind derived quantities are explained and references to detailed treatments are provided where possible. The content and presentation style of the beginning portions of this document are heavily inspired by Daniel Steck's excellent unpublished resources on ^{133}Cs and ^{23}Na [2, 3], while the later half draws on the exposition of scattering presented in a thesis by Ken O'Hara [4].

2 Copyright and License Information

Version	Date	Changed By	Version Info
1.0	Feb. 25, 2003	Michael Gehm	Appendix to thesis
1.1	Sep. 26, 2003	Michael Gehm	Standalone version, fixed typos

Table 1: Revision history of this document.

Property	Symbol	Value	Ref.
Density (300 K)	ρ	$0.534\,\mathrm{g}\cdot\mathrm{cm}^{-3}$	[5]
Melting Point	T_M	453.69 K	[5]
Heat of Fusion	Q_F	$2.99\,\mathrm{kJ}\cdot\mathrm{mol}^{-1}$	[5]
Boiling Point	T_B	1615 K	[5]
Heat of Vaporization	Q_V	$134.7\,\mathrm{kJ}\cdot\mathrm{mol}^{-1}$	[5]

Table 2: Fundamental physical properties of bulk lithium.

3 Fundamental Physical Properties

Lithium, in solid form, is the lightest of the metals and presents a silvery-grey appearance. Like all alkalis, it reacts with water, but not as violently as sodium [5]. The fundamental physical properties of bulk lithium are listed in Table 2. The concentration on thermodynamic properties is indicative of the fact that in atomic cooling and trapping experiments, the bulk element is only used as a consumable for the atomic source. In addition to the numerical data in the table, there is one more important bulk property—vapor pressure. The atomic number density is directly related to the vapor pressure and is the primary adjustable parameter for a given atomic-beam or vapor-cell atom source. The vapor pressure of lithium in the solid and liquid phases is given by [6]

$$\begin{aligned}\log_{10} P_{V_{sol}} &= -54.87864 - \frac{6450.944}{T} - 0.01487480\,T + 24.82251\,\log_{10} T\,,\\ \log_{10} P_{V_{liq}} &= 10.34540 - \frac{8345.574}{T} - 0.00008840\,T - 0.68106\,\log_{10} T\,.\end{aligned}$$

Above, pressure is in Torr (mm Hg) and temperature is in Kelvin. A plot of the vapor pressure over temperature ranges relevant to our experiment is shown in Figure 1.

Lithium appears naturally in two stable isotopes. ^{7}Li with four neutrons, and ^{6}Li with three. Since the two isotopes differ by a single spin-$1/2$ particle, they exhibit different quantum statistics. ^{7}Li is a composite boson, while ^{6}Li is a composite fermion. This thesis is solely concerned with the fermionic isotope. The fundamental physical properties of ^{6}Li in its atomic form are shown in Table 3

4 Optical Properties

Like all alkalis, the optical spectrum of lithium contains a prominent spectroscopic feature, called the D-line for historical reasons. It is fairly easy to discern that this line consists of two narrowly separated features, logically named the D_1 (redmost) and D_2 lines. The physical principles underlying the two components and their, as yet unmentioned, internal structure will be briefly discussed in the next section. Some basic properties of the D_1 and D_2 transitions in ^{6}Li are listed in Table 4 and Table 5, respectively.

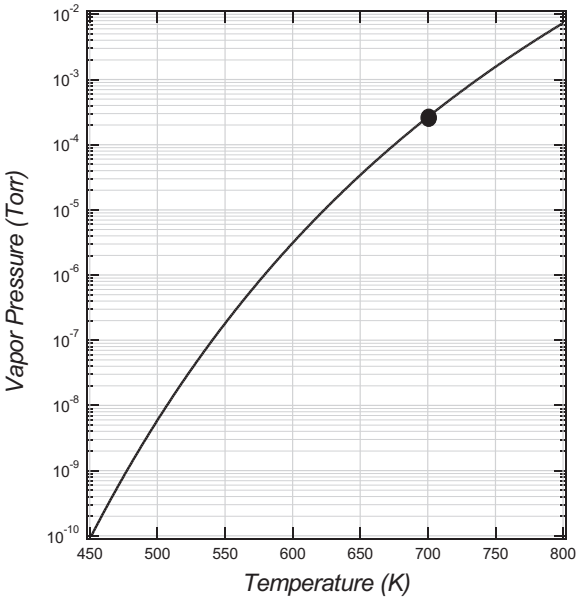

Figure 1: Vapor pressure of ^{6}Li. The melting point of ^{6}Li occurs at the left axis. The circle marks the approximate operating point of our atomic source.

Property	Symbol	Value	Ref.
Atomic Number	Z	3	
Nucleons	$Z+N$	6	
Natural Abundance	η	7.6%	[5]
Nuclear Lifetime	τ_n	stable	[5]
Atomic Mass	m	$6.015\,121\,4\,\mathrm{u}$ $9.988\,341\,4\times10^{-27}\,\mathrm{kg}$	[7]
Total Electronic Spin	S	$1/2$	
Total Nuclear Spin	I	1	

Table 3: Fundamental physical properties of atomic ^{6}Li.

Property	Symbol	Value	Ref.
Wavelength (vacuum)	λ	670.992 477 nm	
Wavenumber (vacuum)	$k/2\pi$	14 903.297 cm^{-1}	
Frequency	ν	446.789 5961 THz	[9]
Lifetime	τ	27.102 ns	[8]
Natural Linewidth	Γ	$36.898 \times 10^6\ \mathrm{s}^{-1}$ 5.872 4 MHz	
Atomic Recoil Velocity	v_{rec}	9.886 554 cm $\cdot$ sec^{-1}	
Recoil Temperature	T_{rec}	3.535 652 56 μK	

Table 4: Optical properties of the D_1 line of ^{6}Li.

The wavenumber, k, wavelength, λ, and the frequency, ν, in the tables are related by the expressions

$$k = \frac{2\pi}{\lambda} \qquad \text{and} \qquad \lambda\nu = c, \tag{1}$$

with c the speed of light in vacuum. It is interesting to note that the excited-state lifetimes for both the D_1 and D_2 lines are identical. This is not typical in the alkalis, however, for ^{6}Li the difference in the two lifetimes is within the uncertainty of the most precise measurement to date [8]. The natural linewidth of the the optical transitions is inversely related to the excited state lifetime,

$$\Gamma = \frac{1}{\tau}. \tag{2}$$

The recoil velocity is the velocity associated with the momentum of a single resonant photon absorption or emission. It is easily calculated from

$$m v_{rec} = p_{rec} = \hbar k. \tag{3}$$

For atomic cooling and trapping experiments, it is customary to convert many parameters to temperature *units* (noting that the resulting values, since they do not represent equilibrium energy distributions, are not, strictly speaking, temperatures). The recoil velocity is converted to a recoil temperature by relating the kinetic and thermal energies:

$$\frac{1}{2}\, m\, v_{rec}^2 = k_b\, T_{rec}. \tag{4}$$

This shows that, were it possible for a ^{6}Li atom to be perfectly at rest, the absorption or emission of a single resonant photon will give the atom a speed comparable to atomic speeds in a gas of ^{6}Li at $\simeq 3.5\,\mu$K. Clearly, for an ultracold gas of ^{6}Li at $T_{\mathrm{gas}} \leq 1\,\mu$k (not unusual for a degenerate or near-degenerate sample), heating of this magnitude is to be avoided!

Property	Symbol	Value	Ref.
Wavelength (vacuum)	λ	670.977 380 nm	
Wavenumber (vacuum)	$k/2\pi$	14 903.632 cm^{-1}	
Frequency	ν	446.799 6489 THz	[9]
Lifetime	τ	27.102 ns	[8]
Natural Linewidth	Γ	$36.898 \times 10^6\ \mathrm{s}^{-1}$ 5.872 4 MHz	
Atomic Recoil Velocity	v_{rec}	9.886 776 cm $\cdot$ sec^{-1}	
Recoil Temperature	T_{rec}	3.535 811 52 μK	

Table 5: Optical properties of the D_2 line of ^{6}Li.

5 Fine and Hyperfine Structure

^{6}Li has a single, unpaired valence electron. The ground state configuration is $1s^2\,2s^1$; while the excited state configuration is $1s^2\,2p^1$. The simplest view of the energy levels of ^{6}Li, the *central-field approximation*, takes only this fact into account, and computes the energy of the atom assuming that the valence electron is independent, and that the nucleus and closed electron shell produce a spherically-symmetric electric field. The resulting ground and excited states are schematically indicated in the leftmost column of Figure 2. The transition between these two states is responsible for the broad structure of the spectroscopic D-line. The ground and excited levels are given the spectroscopic notation $2\,^2S$ and $2\,^2P$, respectively.

The two sub-features of the D-line, the D_1- and D_2-lines, result from the interaction between the intrinsic angular momentum (spin) of the valence electron and the angular momentum of its orbit. This interaction is known, naturally enough, as the *spin-orbit* coupling, and the splitting of the D-line into the D_1- and D_2-lines is the *fine structure*. Physically, the fact that there is an energy contribution from the interaction of the two angular momenta can be understood by considering the *gyromagnetic ratios* (*g-factors*). The g-factors describe the fact that a charged particle with angular momentum naturally gives rise to a magnetic dipole moment—the g-factor is the constant of proportionality between the the two quantities. So the orbital angular momentum produces a magnetic dipole moment, as does the electron spin. There is an interaction energy between two dipole moments, however, and hence a contribution to the Hamiltonian. The interaction can be written as [10]:

$$\hat{H}'_{SO} = \frac{e}{2m^2c^2\hbar^2}\left[\frac{1}{r}\frac{d\Phi}{dr}\right]\hat{\mathbf{L}}\cdot\hat{\mathbf{S}} \equiv f(r)\,\hat{\mathbf{L}}\cdot\hat{\mathbf{S}}, \tag{5}$$

where $\hat{\mathbf{L}}$ and $\hat{\mathbf{S}}$ are the orbital angular momentum and spin operators, respectively. ϕ is the electric potential produced by the nucleus and the inner electrons, and r is the radial coordinate. In computing the value of this perturbation Hamiltonian, it is convenient to work in the total electronic angular momentum, $\hat{\mathbf{J}}$, basis. We define a new operator

$$\hat{\mathbf{J}} = \hat{\mathbf{L}} + \hat{\mathbf{S}}. \tag{6}$$

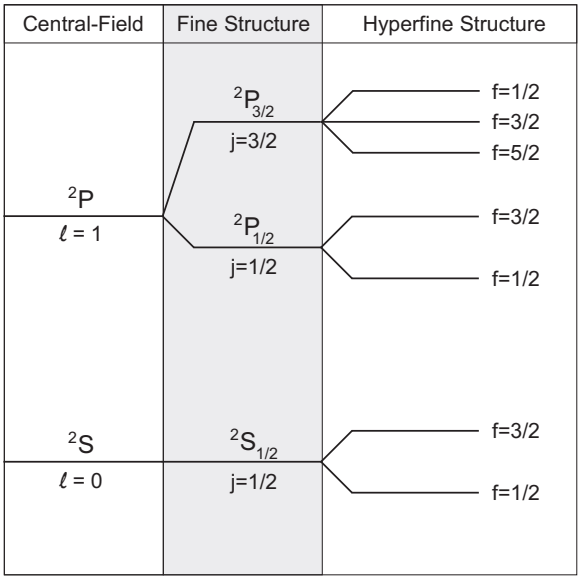

Figure 2: Ground (lower) and first excited (upper) states of ^{6}Li in the L, J, and F bases. The states are also labelled with spectroscopic notation where appropriate. Energy splittings are not to scale.

The quantum-number J can then take on values in integral steps in the range

$$|L - S| \leq J \leq (L + S). \tag{7}$$

We can then make use of the identity

$$\hat{J}^2 = \hat{L}^2 + \hat{S}^2 + 2\,\hat{\mathbf{L}} \cdot \hat{\mathbf{S}}, \tag{8}$$

to write the interaction in (5) in terms of the operators $\hat{J}^2$, $\hat{L}^2$, and $\hat{S}^2$ which, along with $\hat{J}_z$ form a complete set of commuting operators.

Let us now apply this knowledge to the ground and excited states of ^{6}Li. The ground state has $S = 1/2$ and $L = 0$. This implies a single value for J, namely $J = 1/2$. The excited state, however, has $S = 1/2$ and $L = 1$. There are two possible values for J, $J = 1/2\,, 3/2$. Thus, the spin-orbit interaction splits the excited state into two. The state with $J = 1/2$ is given the spectroscopic name $2\,^2P_{1/2}$ and the state with $J = 3/2$ is named $2\,^2P_{3/2}$. The effect of the spin-orbit interaction is schematically indicated in the middle column of Figure 2. We see now that the D_1-line is the spectroscopic feature that results from $2\,^2S_{1/2} \leftrightarrow 2\,^2P_{1/2}$ transitions and the D_2-line results from $2\,^2S_{1/2} \leftrightarrow 2\,^2P_{3/2}$ transitions. The g-factors for electron spin and $L = 1$ electron orbit, along with an experimental measurement of the fine-structure splitting, is given in Table 6.

In the previous section, allusions were made to substructure within the D_1- and D_2-lines. This is known as the *hyperfine structure*, and results from the fact that the atomic nucleus is not truly spherically symmetric as we have assumed up to this point. Rather than consider the interaction energy of the valence electron in an asymmetric field from the nucleus, we consider the equivalent interaction energy of an asymmetric nucleus in the field of the valence

Property	Symbol	Value	Ref.
Electron Spin g-factor	g_S	2.002 319 304 373 7	[11]
Electron $L = 1$ Orbital g-factor	g_L	0.999 995 87	
$2P$ Fine Structure Splitting	ΔE_{FS}	10.052 779 GHz	[9]

Table 6: Electron g-factors and fine-structure splitting for ^{6}Li.

electron. In such a framework, the interaction Hamiltonian is given by [12]:

$$\hat{H}'_{HF} = -\hat{\boldsymbol{\mu}} \cdot \hat{\mathbf{B}}(0) + \frac{1}{6}\, e \sum_{\alpha\beta} \hat{Q}_{\alpha\beta} \frac{\partial^2 \phi(0)}{\partial x_\alpha \partial x_\beta}, \tag{9}$$

where $\hat{\boldsymbol{\mu}}$ and $\hat{Q}$ are the nuclear magnetic dipole moment and nuclear electric quadrupole moment operators respectively. $\hat{\mathbf{B}}$ is the magnetic field operator at the location of the nucleus, and ϕ is the electric potential at the nucleus. The first term is a magnetic dipole interaction, and as such, is analogous to the spin-orbit interaction discussed previously. The second term is an electric quadrupole interaction and only contributes when the valence electron is in a state that has a non-spherically-symmetric electric field. Of the states we have considered, the $2\,^2S_{1/2}$ state arises from an orbital state with $L = 0$. As such, its angular wavefunction is given by a spherical harmonic Y_0^0, which is spherically symmetric. Additionally, the $2\,^2P_{1/2}$ state transitions to the ground state with only zero or one unit of transferred angular momentum, and as such can not support a quadrupole interaction with two units of angular momentum. Only the $2\,^2P_{3/2}$ can support such a interaction, and as a result, only it has a non-zero electric quadrupole contribution.

To incorporate this interaction, it becomes convenient to work in the total atomic angular momentum, $\hat{\mathbf{F}}$, basis. We define

$$\hat{\mathbf{F}} = \hat{\mathbf{J}} + \hat{\mathbf{I}}, \tag{10}$$

where $\hat{\mathbf{I}}$ is the total nuclear angular momentum operator, analogous to $\hat{\mathbf{J}}$ for electrons. The quantum number F can take on values in integral steps in the range

$$|J - I| \leq F \leq (J + I). \tag{11}$$

We can then make use of an identity analogous to (8) to express the interaction in terms of $\hat{F}^2$, $\hat{J}^2$, and $\hat{I}^2$, which, along with $\hat{F}_z$, again form a complete set of commuting operators. In this new basis, the interaction is given by [12]

$$\Delta E_{HF} = \frac{1}{2}\, A\, C + \frac{3}{8}\, B\, \frac{C(C+1)}{I\,(2I-1)\,J\,(2J-1)}, \tag{12}$$

where $C = F(F+1) - J(J+1) - I(I+1)$, and A and B are the *magnetic dipole hyperfine constant* and *electric quadrupole hyperfine constant*, respectively for the F state of interest. Experimental measurements of the hyperfine constants of ^{6}Li are listed in Table 7.

Applying these concepts to the fine-structure levels, we see that the $2\,^2S_{1/2}$ level with $J = 1/2$ and $I = 1$ (see Table 3) has two possible values of F: $F = 1/2\,, 3/2$. The $2\,^2P_{1/2}$

Property	Symbol	Value	Ref.
$2\,^2S_{1/2}$ Magnetic Dipole Constant	$A_{2\,^2S_{1/2}}$	152.136 840 7 MHz	[13]
$2\,^2P_{1/2}$ Magnetic Dipole Constant	$A_{2\,^2P_{1/2}}$	17.386 MHz	[14]
$2\,^2P_{3/2}$ Magnetic Dipole Constant	$A_{2\,^2P_{3/2}}$	-1.155 MHz	[13]
$2\,^2P_{3/2}$ Electric Quadrupole Constant	$B_{2\,^2P_{3/2}}$	-0.10 MHz	[13]

Table 7: Hyperfine constants for the $2S$ and $2P$ levels of lithium.

state also has possible F-values of $F = 1/2\,, 3/2$. The $2\,^2P_{3/2}$ state, however, has the possible values $F = 1/2\,, 3/2, 5/2$. This splitting is indicated schematically in the rightmost column of Figure 2.

At this point, we have essentially described the structure of the ground and $2P$ excited states of ^{6}Li in a region free of external fields. The results are summarized in a level diagram in Figure 3. In the next section, we address the application of external fields.

6 Interaction With DC Fields

6.1 Magnetic Fields

The tuning of atomic levels in static magnetic field is known as the *Zeeman* effect. As we have previously noted, a charged particle with angular momentum is a magnetic dipole. Any such dipole will have an interaction energy in an applied magnetic field. The interaction Hamiltonian is quite simple, and is given by

$$\hat{H}_B = -\frac{\mu_B}{\hbar} \sum_x g_x \, \hat{\mathbf{X}}_z \cdot \hat{\mathbf{B}} \tag{13}$$

where the sum is over *good angular momentum quantum numbers*, and g_x and $\hat{X}_z$ are the g-factor and angular momentum projection operator corresponding to those numbers.

As the B-field increases from zero, the Zeeman interaction is initially small compared to the hyperfine interaction. Thus, we may treat it as a perturbation to the hyperfine levels we derived earlier. In this case, $\mathbf{F}$ precesses around $\mathbf{B}$, hence F is still a good quantum number, and (13) reduces to

$$\Delta E_z = \frac{\mu_B}{\hbar} g_F m_F B. \tag{14}$$

The g-factor, g_F, is given by a *Landé g-factor* expression that combines g_J and g_I

$$g_F = g_J \frac{F(F+1) - I(I+1) + J(J+1)}{2F(F+1)} + g_I \frac{F(F+1) + I(I+1) - J(J+1)}{2F(F+1)}. \tag{15}$$

Values of g_J and g_I are given in Table 8. In this regime, the energies tune linearly with B. In alkalis, this region is known as the *anomalous Zeeman effect*. "Anomalous" because the spectral lines split into doublets, quadruplets, and sextuplets, rather than triplets as

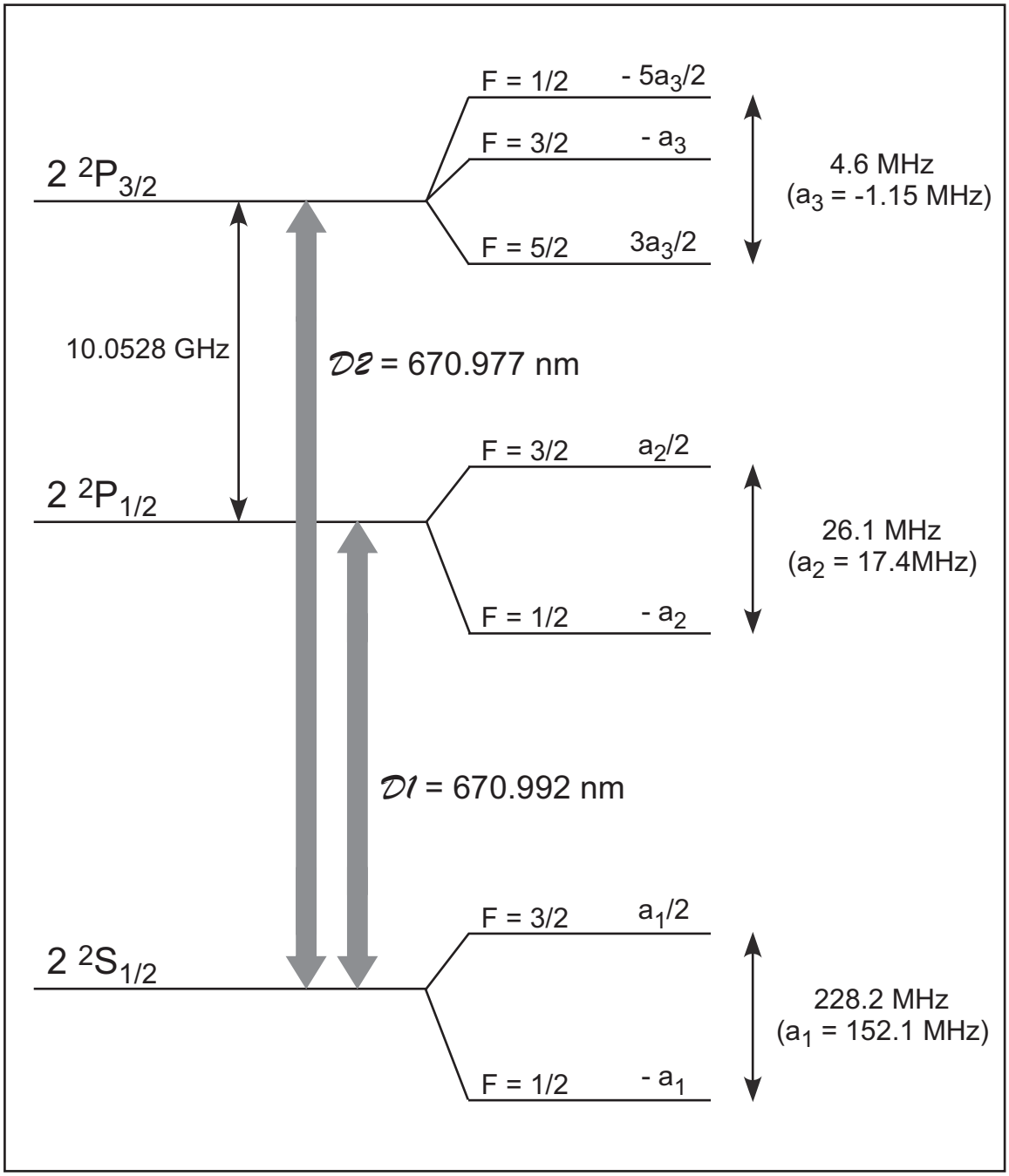

Figure 3: Level diagram of the ground and 2P excited states of ^{6}Li. Energy splittings are not to scale.

Property	Symbol	Value	Ref.
Total Nuclear g-factor	g_I	-0.000 447 654 0	[13]
Total Electronic g-factor	$g_J\,(2\,^2S_{1/2})$	2.002 301 0	[13]
	$g_J\,(2\,^2P_{1/2})$	0.666 8	[13]
	$g_J\,(2\,^2P_{3/2})$	1.335	[13]

Table 8: Total nuclear and total electronic g-factors for ^{6}Li.

predicted by a semiclassical theory of Lorenz (his theory was developed prior to knowledge of spin—as such, only atoms with total spin $S = 0$ exhibit the *normal Zeeman effect* at low field).

Eventually, the magnetic energy becomes significant compared to the hyperfine energy. When this happens, the Zeeman effect can no longer be treated as a perturbation. At this point, $\mathbf{F}$ ceases to be a good description of the system, and F is no longer a good quantum number. We are now forced to find eigenstates of the combined interaction Hamiltonian

$$\hat{H}_{int} = \hat{H}_B + \hat{H}_{HF} = \frac{\mu_B}{\hbar}\sum_x g_x\,\hat{\mathbf{X}}\cdot\hat{\mathbf{B}} - \hat{\boldsymbol{\mu}}\cdot\hat{\mathbf{B}}(0) + \frac{1}{6}\,e\sum_{\alpha\beta}\hat{Q}_{\alpha\beta}\frac{\partial^2\phi(0)}{\partial x_\alpha \partial x_\beta}. \tag{16}$$

This region occurs at very low fields for ^{6}Li. The ground and excited states have extremely small hyperfine splittings compared to other alkalis. As a result, the combined interaction Hamiltonian must be used for fields as small as a few Gauss. Finding the eigenstates is, of course, a matter of diagonalizing the Hamiltonian. While this is generally done numerically, it has been done analytically for the hyperfine ground states of ^{6}Li [15]. Expressed in the $|m_S\ m_I\rangle$ basis, the authors find the eigenstates to be

$$\begin{aligned}
|1\rangle &= \sin\theta_+\,|1/2\ \ 0\rangle - \cos\theta_+\,|-1/2\ \ 1\rangle \\
|2\rangle &= \sin\theta_-\,|1/2\ \ -1\rangle - \cos\theta_-\,|-1/2\ \ 0\rangle \\
|3\rangle &= |-1/2\ \ -1\rangle \\
|4\rangle &= \cos\theta_-\,|1/2\ \ -1\rangle + \sin\theta_-\,|-1/2\ \ 0\rangle \\
|5\rangle &= \cos\theta_+\,|1/2\ \ 0\rangle + \sin\theta_+\,|-1/2\ \ 1\rangle \\
|6\rangle &= |1/2\ \ 1\rangle
\end{aligned} \tag{17}$$

where the states are numbered in order of increasing energy. In the above, $\sin\theta_\pm = 1/\sqrt{1+(Z^\pm+R^\pm)^2/2}$, $\cos\theta_\pm = \sqrt{1-\sin\theta_\pm}$, $Z^\pm = (\mu_n + 2\mu_e)B/A_{2\,^2S_{1/2}} \pm 1/2$, and $R^\pm = \sqrt{(Z^\pm)^2+2}$. Also note that m_J has been replaced with m_S since $L = 0$ for the ground state.

Numerical results for the $2\,^2S_{1/2}$, $2\,^2P_{1/2}$, and $2\,^2P_{3/2}$ states are shown in Figures 4, 5, and 6, respectively. The numerical results for the $2\,^2S_{1/2}$ state are identical to those obtained from the analytical results above. The computer code that generated these results can be found in [1].

As the field strength continues to grow, eventually the hyperfine energy can be neglected and the eigenstates are those of the Zeeman Hamiltonian. At this point, we can treat the

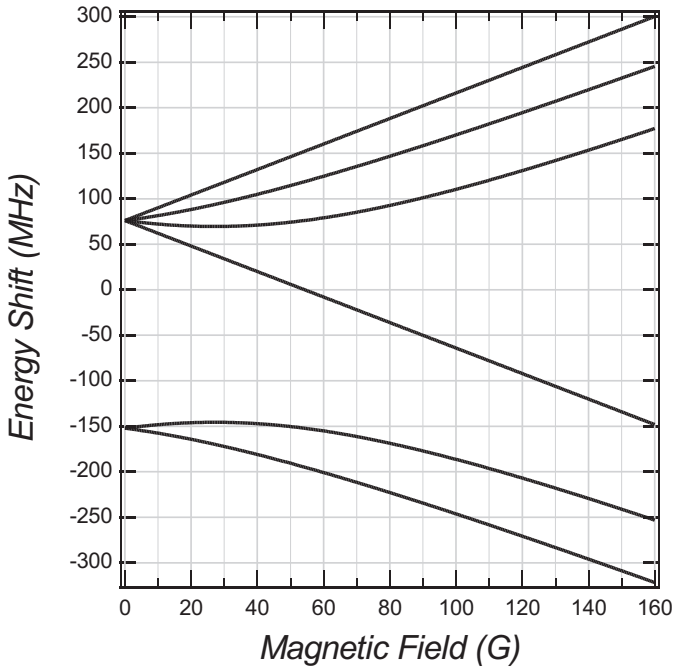

Figure 4: Magnetic-field dependence of the $2\,^2S_{1/2}$ ground state of ^{6}Li.

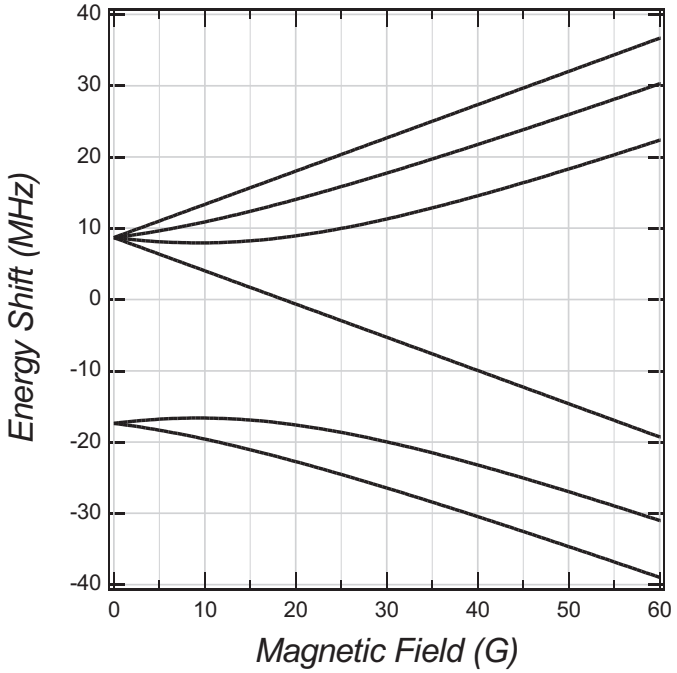

Figure 5: Magnetic-field dependence of the $2\,^2P_{1/2}$ excited state of ^{6}Li.

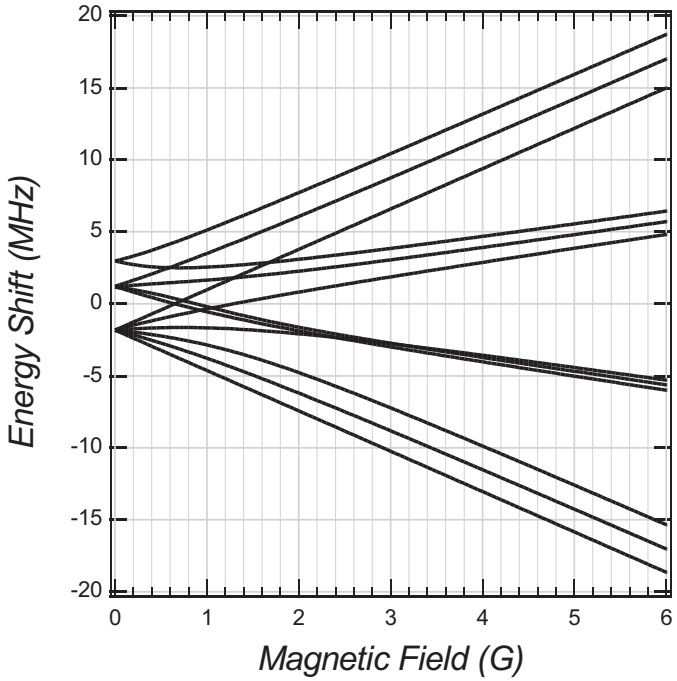

Figure 6: Magnetic-field dependence of the $2\,^2P_{3/2}$ excited state of ^{6}Li.

atoms in a pure product state basis $|Jm_J\rangle\,|Im_I\rangle$. Each ket is treated independently with respect to the Zeeman effect—in other words (13) becomes:

$$\Delta E_z = \frac{\mu_B}{\hbar}(g_J m_J + g_I m_I)B. \tag{18}$$

At this point, the states are arranged into spectroscopic triplets (the normal Zeeman effect). Further, since $g_J \gg g_I$, for sufficiently large fields, the nuclear contribution can be neglected, and the energies are well approximated by

$$\Delta E_z \simeq \frac{\mu_B}{\hbar} g_J m_J B. \tag{19}$$

Of course, the numerical treatment of the complete Hamiltonian captures this behavior as well—note the organization of the levels into triplets in the high-field regions of Figures 4, 5, and 6.

Eventually, the magnetic interaction will become significant with respect to the spin-orbit interaction. The two energies become comparable at fields on the order of 1 T=10 000 G. As a result, precision calculations must cease using the J-basis for field-strengths in excess of about 500-1000 G. Future experiments in our laboratory will place the atoms in field-strengths as large as 1200 G. To treat this problem, the atoms are described in the $|S\ m_S\rangle\,|L\ m_L\rangle\,|I\ m_I\rangle$ product basis, and the combined spin-orbit and Zeeman Hamiltonian is diagonalized (the excited state hyperfine interaction is neglected because of its relatively small contribution). The results of this calculation for the L=1 excited state are shown in Figure 7.

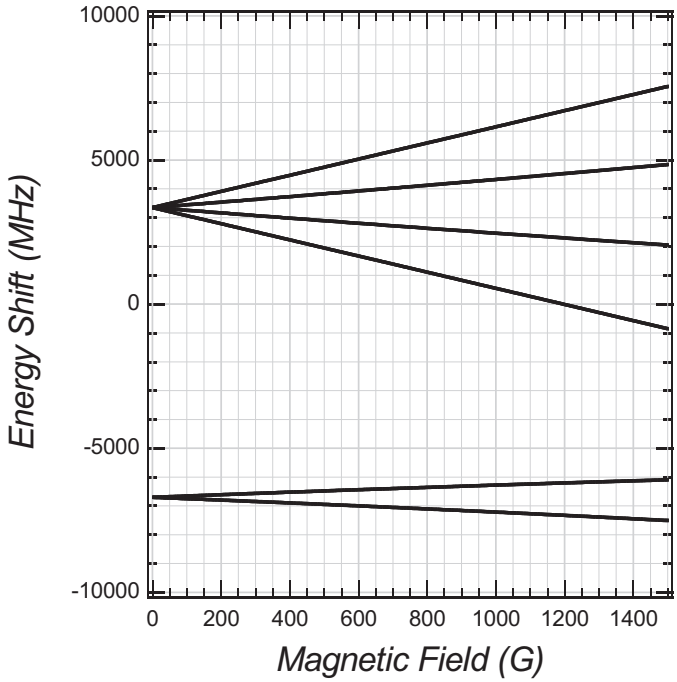

Figure 7: High-field Zeeman splitting of the D_1 and D_2 excited states of ^{6}Li. The hyperfine contribution has been neglected in this calculation. The size of the nuclear contribution is negligible on this scale; as a result, each line is three-fold degenerate.

6.2 Electric Fields

The interaction between an atom and a DC electric field is known as the *Stark effect* and is substantially simpler than the Zeeman effect. The interaction is described in the $\hat{\mathbf{J}}$-basis, and the interaction energy is given by [16]:

$$\Delta E_m = -1/2 \;\alpha(m)\,\mathcal{E}^2 \tag{20}$$

where $\alpha(m)$ is the static polarizability of the atom in a magnetic sublevel m, and $\mathcal{E}$ is the electric field strength. By using irreducible tensor operators, it can be shown that the static polarizability can always be written in terms of a scalar polarizability α_0 and a tensor polarizability α_2 [17]:

$$\alpha(m) = \alpha_0 + \alpha_2 \frac{3m^2 - J\,(J+1)}{J\,(2J-1)} \quad . \tag{21}$$

Table 9 list the static and tensor polarizabilities for the $2\,^2S_{1/2}$, $2\,^2P_{1/2}$, and $2\,^2P_{3/2}$ levels of ^{6}Li. The tensor polarizability is rank 2, and as we saw before, only the $2\,^2P_{3/2}$ level can support such an operator. Hence, only that state has a tensor polarizability.

If we consider the atom in the $\hat{\mathbf{F}}$-basis, for small enough electric fields, the Stark interaction can be treated as a perturbation on the the hyperfine eigenstates. What is small enough? Well, if we consider an effect of $\simeq 5\%$ of the hyperfine energy as where a perturbation stops being small, then we can write the corresponding electric field strength as:

$$\mathcal{E}^2_{max} \;\simeq\; 2\,(0.05)\,\frac{A_J}{\alpha_{0_J}} \tag{22}$$

Property	Symbol	Value	Ref.
$2\,^2S_{1/2}$ Scalar Polarizability	$\alpha_0\ (2\,^2S_{1/2})$	$0.040\,8\,\mathrm{Hz/(V/cm)^2}$	[18]
$2\,^2P_{1/2}$ Scalar Polarizability	$\alpha_0\ (2\,^2P_{1/2})$	$0.031\,56\,\mathrm{Hz/(V/cm)^2}$	[19]
$2\,^2P_{3/2}$ Scalar Polarizability	$\alpha_0\ (2\,^2P_{3/2})$	$0.031\,63\,\mathrm{Hz/(V/cm)^2}$	[19]
$2\,^2P_{3/2}$ Tensor Polarizability	$\alpha_2\ (2\,^2P_{3/2})$	$0.000\,406\,\mathrm{Hz/(V/cm)^2}$	[19]

Table 9: D-line polarizabilities of ^{6}Li.

where A_J is the magnetic dipole hyperfine constant for the appropriate fine structure state (found in Table 7). From this, we see that in the ground state, a perturbation treatment is acceptable up to a field strength of approximately 19.5 kV/cm! For the states in the $2\,^2P_{1/2}$ and $2\,^2P_{3/2}$ manifolds, we get values of 7.4 kV/cm and 1.9 kV/cm, respectively.

In this regime, the eigenstates remain eigenstates of the $\hat{\mathbf{F}}$-basis, and we shift the energies of the levels according to (20) and (21). If we are interested in field strengths outside this range, then we must include both the Stark effect (20) and the hyperfine interaction (12) in our Hamiltonian, and diagonalize the resulting matrix. Eventually, of course, the Stark effect dominates the hyperfine interaction, and we can work solely with the Stark Hamiltonian.

For realistic experiments, we never have to consider a Hamiltonian that contains the Stark effect and the spin-orbit interaction. Using an equation analogous to (22) to calculate the range over which the Stark effect is a perturbation on the fine structure, we find that it takes fields greater than 170 kV/cm before this becomes an issue.

It is important to note that the predominant result of the Stark effect is an overall energy shift that is quadratic in the electric field. Only the $2\,^2P_{3/2}$ state, with a nonzero tensor polarizability, has a change in the relative splitting of its hyperfine constituents. A plot of this splitting, with the overall quadratic shift suppressed, is shown in Figure 8. The computer code that produced these results can be found in [1].

7 Interaction With Near-Resonant Light

7.1 Optical Transition Matrix Elements

The interaction between the internal states of the atom and an external, near-resonant optical field is quantified through the *electric-dipole transition matrix elements*. These matrix elements describe how the internal states of the atom couple to one another via an electric-dipole ($-\boldsymbol{\mu}\cdot\mathbf{E}$) interaction with the near-resonant field [20] (magnetic transitions and transitions of higher multipolar order exist, but are substantially weaker than the electric-dipole transition). If we start in a hyperfine state represented by $|(JI)Fm_F\rangle$ and couple to a state $\left|(J'I')F'm_{F'}\right\rangle$, then the matrix element for this transition is given by $\left\langle(J'I')F'm_{F'}\right|\ \hat{\boldsymbol{\mu}}\ \left|(JI)Fm_F\right\rangle$, where $\hat{\boldsymbol{\mu}}$ is the electric-dipole operator. We can use the *Wigner-Eckart Theorem* [21] to represent this matrix element in terms of a *reduced* matrix element that is m-independent. Recognizing that we can write the electric-dipole operator, $\hat{\boldsymbol{\mu}}$ as an irreducible spherical tensor operator, $\hat{\mu}(k,q)$, with $k=1$ and $q=-1,0,1$ for

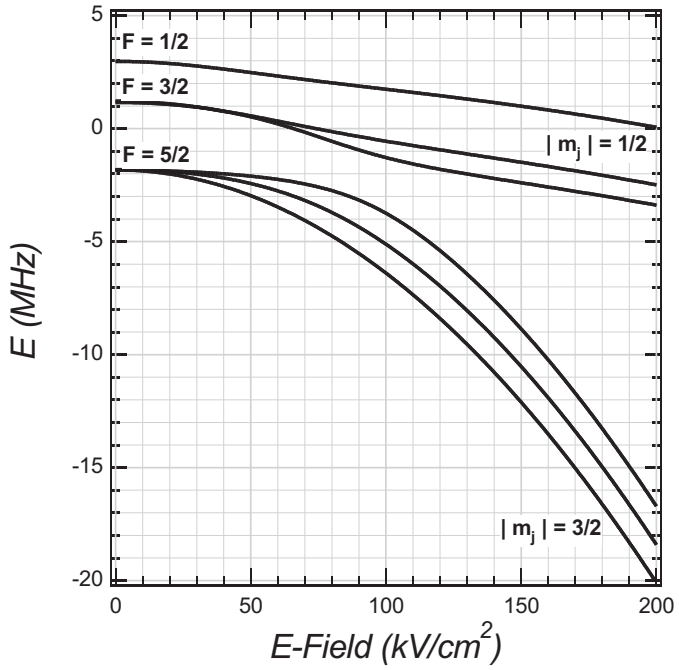

Figure 8: Stark-effect shifts of the $2\,^2P_{3/2}$ level of ^{6}Li. An overall shift proportional to $\mathcal{E}^2$ has been suppressed.

electric-dipole radiation with σ^-, π, and σ^+ polarization respectively, we can directly use the Wigner-Eckart theorem to write [22]:

$$\left\langle (J'I')F'm_{F'} \left| \hat{\mu}(1,q) \right| (JI)Fm_F \right\rangle = (-1)^{F'-m_{F'}} \begin{pmatrix} J' & 1 & J \\ -m_{F'} & q & m_F \end{pmatrix} \times \left\langle (J'I')F' \left\| \hat{\mu}(1) \right\| (JI)F \right\rangle . \quad (23)$$

The reduced matrix element is written with double vertical bars for easy identification. The factor in parenthesis is known as a *Wigner 3-J Symbol* [21], and describes the magnetic-quantum-number-dependence of the matrix element. Most notably, it is identically zero unless $m_{F'} = m_F + q$ and $F' = F \pm 1$. Thus, it automatically enforces the appropriate selection rules.

We can further reduce the expression through the use of *angular momentum recoupling* [21]. Although a transition between two F-states changes F, it does so by changing J and leaving I unchanged. We can rewrite our reduced matrix element in a manner that makes the J-changing nature of the transition more apparent [22]:

$$\left\langle (J'I')F' \left\| \hat{\mu}(1) \right\| (JI)F \right\rangle = \delta_{I'I} \, (-1)^{J'+I+F+1} \sqrt{(2F'+1)(2F+1)} \times \begin{Bmatrix} J' & I & F' \\ F & 1 & J \end{Bmatrix} \left\langle J' \left\| \hat{\mu}(1) \right\| J \right\rangle . \quad (24)$$

The term in the large braces is a *Wigner 6-J Symbol* [21]. We can combine (23) and (24) to

achieve the final result:

$$\left\langle (J^{'}I^{'})F^{'}m_{F^{'}} \left| \hat{\mu}(1,q) \right| (JI)Fm_F \right\rangle = \delta_{I^{'}I}\,(-1)^{F^{'}+F+J^{'}+I-m_{F^{'}}+1}\sqrt{(2F^{'}+1)(2F+1)}\times \begin{pmatrix} J^{'} & 1 & J \\ -m_{F^{'}} & q & m_F \end{pmatrix} \begin{Bmatrix} J^{'} & I & F^{'} \\ F & 1 & J \end{Bmatrix} \times \left\langle J^{'} \left\| \hat{\mu}(1) \right\| J \right\rangle . \quad (25)$$

It is hard to over-emphasize the importance of (25). A moment of reflection will show that for the states we have been considering, there are only two possible values of $\left\langle J^{'} \left\| \hat{\mu}(1) \right\| J \right\rangle$—one for the D_1-line and one for the D_2-line! To calculate the transition strength between two F-levels, one merely has to determine whether the transition belongs to the D_1- or D_2-line and multiply the appropriate reduced matrix element by the prefactors of (25).

But what are the values of the reduced matrix elements? We can make a step towards answering this question by once again employing angular momentum recoupling. The total electronic angular momentum J is comprised of the orbital angular momentum L and the spin S. The electric dipole transition only changes L, so we can explicitly extract this L-changing nature of the transition. In analogy with (24):

$$\left\langle (L^{'}S^{'})J^{'} \left\| \hat{\mu}(1) \right\| (LS)J \right\rangle = \delta_{S^{'}S}\,(-1)^{L^{'}+S+J+1}\sqrt{(2J^{'}+1)(2J+1)}\times \begin{Bmatrix} J^{'} & I & F^{'} \\ F & 1 & J \end{Bmatrix} \left\langle L^{'} \left\| \hat{\mu}(1) \right\| L \right\rangle . \quad (26)$$

Now we have a single reduced matrix element that corresponds to the entire D-line. The value of this matrix element and of the D_1 and D_2 matrix elements are given in Table 10. The prefactors in (25) have been tabulated for all transitions in the D_1- and D_2-lines. The results are shown in Tables 11, 12, and 13. The computer code that generated these values can be found in [1].

7.2 Transition Matrix Element Sum Rules

The tables of transition matrix elements exhibit several interesting *sum rules* as a result of the symmetrical nature of the electric dipole operator. These rules can be simply derived from the mathematical properties of the 3- and 6-J symbols [21].

We begin by considering the sum of the squares of the matrix elements for transitions from a single magnetic sublevel, m_F, in a single level, F, to all magnetic sublevels in a single level, $F^{'}$, via all possible polarizations:

$$\begin{aligned} S_{F,\,F^{'}} &= \sum_q \left| \left\langle (J^{'}I^{'})F^{'}\,(m_F+q) \left| \hat{\mu}(1,q) \right| (JI)F\,m_F \right\rangle \right|^2 \\ &= (2F^{'}+1) \begin{Bmatrix} J^{'} & I & F^{'} \\ F & 1 & J \end{Bmatrix}^2 \left| \left\langle J^{'} \left\| \hat{\mu}(1) \right\| J \right\rangle \right|^2 . \end{aligned} \quad (27)$$

Note the result does not depend on m_F. Therefore the result is independent of what magnetic sublevel we start in. The values of $S_{F,\,F^{'}}$ reflect the relative strength of transitions between different F-levels. These values are tabulated in Table 14.

Property	Symbol	Value	Ref.
D-Line Reduced Matrix Element	$\left\langle L' = 1 \left\| \hat{\mu}(1) \right\| L = 0 \right\rangle$	1.148×10^{-29} C·m 3.443×10^{-18} esu·cm 3.443 Debye $\sqrt{3}\,\mu_0$	
D_1-Line Reduced Matrix Element	$\left\langle J' = 1/2 \left\| \hat{\mu}(1) \right\| J = 1/2 \right\rangle$	-2.812×10^{-29} C·m -8.433×10^{-18} esu·cm -8.433 Debye $-\sqrt{2}\,\mu_0$	
D_2-Line Reduced Matrix Element	$\left\langle J' = 3/2 \left\| \hat{\mu}(1) \right\| J = 1/2 \right\rangle$	3.977×10^{-29} C·m 11.925×10^{-18} esu·cm 11.925 Debye $2\,\mu_0$	

Table 10: Reduced matrix elements for ^{6}Li.

If we then sum over final F-levels, we derive the rule of primary physical importance:

$$\begin{aligned} \sum_{F'} S_{F,F'} &= \sum_{F',q} \left| \left\langle F'\,(m_F + q) \left| \hat{\mu}(1,q) \right| F\, m_F \right\rangle \right|^2 \\ &= \frac{1}{2J+1} \left| \left\langle J' \left\| \hat{\mu}(1) \right\| J \right\rangle \right|^2 . \end{aligned} \tag{28}$$

While this rule holds for both absorption and emission, the physical implication is most important for emission: *all excited states in a given line (D_1 or D_2) have the same transition strength, and hence decay at the same rate.* In fact, we can relate this result to the decay rate via the *Einstein A-Coefficient* [23]:

$$\begin{aligned} \frac{1}{\tau} &= A_{J,J'} \\ &= \frac{\omega^3}{3\pi\epsilon_0\hbar c^3} \frac{1}{(2J+1)} \left| \left\langle J' \left\| \hat{\mu}(1) \right\| J \right\rangle \right|^2 . \end{aligned} \tag{29}$$

In the above, ϵ_0 is the electric permittivity of free space. With this result, we can take experimentally determined decay rates and transition frequencies and compute the fundamental reduced matrix elements. This is how the values in Table 10 were computed.

7.3 The Photon-Burst Transitions

When we examine the transition matrix elements given in Tables 11, 12, and 13, we discover an interesting fact: the excited states $\left|F' = 5/2\, m_{F'} = \pm 5/2\right\rangle$ each couple to a single ground state, namely $|F = 3/2\, m_F = \pm 3/2\rangle$. When driven by light of the proper polarization (σ^+ for

D_1		$2\,^2P_{1/2}$					
		$F = 3/2$				$F = 1/2$	
		-3/2	-1/2	1/2	3/2	-1/2	1/2
$2\,^2S_{1/2}$	$F = 3/2$						
	-3/2	$-\sqrt{\frac{1}{6}}\,(\pi)$	$-\frac{1}{3}\,(\sigma^+)$			$-\sqrt{\frac{2}{9}}\,(\sigma^+)$	
	-1/2	$\frac{1}{3}\,(\sigma^-)$	$-\sqrt{\frac{1}{54}}\,(\pi)$	$-\sqrt{\frac{4}{27}}\,(\sigma^+)$		$\sqrt{\frac{4}{27}}\,(\pi)$	$-\sqrt{\frac{2}{27}}\,(\sigma^+)$
	1/2		$\sqrt{\frac{4}{27}}\,(\sigma^-)$	$\sqrt{\frac{1}{54}}\,(\pi)$	$-\frac{1}{3}\,(\sigma^+)$	$-\sqrt{\frac{2}{27}}\,(\sigma^-)$	$\sqrt{\frac{4}{27}}\,(\pi)$
	3/2			$\frac{1}{3}\,(\sigma^-)$	$\sqrt{\frac{1}{6}}\,(\pi)$		$-\sqrt{\frac{2}{9}}\,(\sigma^-)$
	$F = 1/2$						
	-1/2	$\sqrt{\frac{2}{9}}\,(\sigma^-)$	$\sqrt{\frac{4}{27}}\,(\pi)$	$\sqrt{\frac{2}{27}}\,(\sigma^+)$		$\sqrt{\frac{1}{54}}\,(\pi)$	$\sqrt{\frac{1}{27}}\,(\sigma^+)$
	1/2		$\sqrt{\frac{2}{27}}\,(\sigma^-)$	$\sqrt{\frac{4}{27}}\,(\pi)$	$\sqrt{\frac{2}{9}}\,(\sigma^+)$	$-\sqrt{\frac{1}{27}}\,(\sigma^-)$	$-\sqrt{\frac{1}{54}}\,(\pi)$

Table 11: D_1-line electric-dipole-transition matrix elements. Results are given in units of $\mu_{D1} = \left\langle J = 1/2 \left\| \hat{\mu}(1) \right\| J' = 1/2 \right\rangle = -\sqrt{2}\mu_0$. The parenthetical terms indicate the polarization of light required to drive the transition.

D_2		$2\,^2P_{3/2}$											
		$F=5/2$											
		$-5/2$		$-3/2$		$-1/2$		$1/2$		$3/2$		$1/2$	
$2\,^2S_{1/2}$	$F=3/2$	$-3/2$	$1/2\ (\sigma^-)$	$-1/2$	$\sqrt{\frac{1}{10}}\ (\pi)$	$-1/2$	$\sqrt{\frac{1}{40}}\ (\sigma^+)$	$1/2$					
		$-1/2$		$1/2\ (\sigma^-)$	$\sqrt{\frac{3}{20}}\ (\pi)$	$1/2$	$\sqrt{\frac{3}{40}}\ (\sigma^+)$	$3/2$					
		$1/2$			$\sqrt{\frac{3}{20}}\ (\sigma^-)$	$3/2$	$\sqrt{\frac{3}{20}}\ (\pi)$	$1/2$	$\sqrt{\frac{3}{40}}\ (\sigma^+)$				
		$3/2$				$1/2$	$\sqrt{\frac{1}{40}}\ (\sigma^-)$	$3/2$	$\sqrt{\frac{1}{10}}\ (\pi)$	$1/2$	$\sqrt{\frac{3}{20}}\ (\sigma^+)$		
	$F=1/2$	$-1/2$											
		$1/2$											

Table 12: D_2-line electric-dipole-transition matrix elements (part1). Results are given in units of $\mu_{D2} = \left\langle J = 1/2 \left\| \hat{\mu}(1) \right\| J' = 3/2 \right\rangle = 2\mu_0$. The parenthetical terms indicate the polarization of light required to drive the transition.

D_2		$2\,^2P_{3/2}$					
		$F = 3/2$				$F = 1/2$	
		$-3/2$	$-1/2$	$1/2$	$3/2$	$-1/2$	$1/2$
$2\,^2S_{1/2}$	$F = 3/2$						
	$-3/2$	$\sqrt{\frac{1}{15}}\,(\pi)$	$\sqrt{\frac{2}{45}}\,(\sigma^+)$			$\sqrt{\frac{1}{72}}\,(\sigma^+)$	
	$-1/2$	$-\sqrt{\frac{2}{45}}\,(\sigma^-)$	$\sqrt{\frac{1}{135}}\,(\pi)$	$\sqrt{\frac{8}{135}}\,(\sigma^+)$		$-\sqrt{\frac{1}{108}}\,(\pi)$	$\sqrt{\frac{1}{216}}\,(\sigma^+)$
	$1/2$		$-\sqrt{\frac{8}{135}}\,(\sigma^-)$	$-\sqrt{\frac{1}{135}}\,(\pi)$	$\sqrt{\frac{2}{45}}\,(\sigma^+)$	$\sqrt{\frac{1}{216}}\,(\sigma^-)$	$-\sqrt{\frac{1}{108}}\,(\pi)$
	$3/2$			$-\sqrt{\frac{2}{45}}\,(\sigma^-)$	$-\sqrt{\frac{1}{15}}\,(\pi)$		$\sqrt{\frac{1}{72}}\,(\sigma^-)$
	$F = 1/2$						
	$-1/2$	$\sqrt{\frac{5}{36}}\,(\sigma^-)$	$\sqrt{\frac{5}{54}}\,(\pi)$	$\sqrt{\frac{5}{108}}\,(\sigma^+)$		$\sqrt{\frac{2}{27}}\,(\pi)$	$\sqrt{\frac{4}{27}}\,(\sigma^+)$
	$1/2$		$\sqrt{\frac{5}{108}}\,(\sigma^-)$	$\sqrt{\frac{5}{54}}\,(\pi)$	$\sqrt{\frac{5}{36}}\,(\sigma^+)$	$-\sqrt{\frac{4}{27}}\,(\sigma^-)$	$-\sqrt{\frac{2}{27}}\,(\pi)$

Table 13: D_2-line electric-dipole-transition matrix elements (part 2). Results are given in units of $\mu_{D2} = \left\langle J = 1/2 \left\| \hat{\mu}(1) \right\| J' = 3/2 \right\rangle = 2\mu_0$. The parenthetical terms indicate the polarization of light required to drive the transition.

Transition Type	$S_{F\,F'}$	Value
D_1 Absorption ($2\,^2S_{1/2} \rightarrow 2\,^2P_{1/2}$)	$S_{1/2\,,\,1/2}$	$1/18$
	$S_{1/2\,,\,3/2}$	$4/9$
	$S_{3/2,\,1/2}$	$2/9$
	$S_{3/2,\,3/2}$	$5/18$
D_1 Emission ($2\,^2P_{1/2} \rightarrow 2\,^2S_{1/2}$)	$S_{1/2\,,\,1/2}$	$1/18$
	$S_{1/2\,,\,3/2}$	$4/9$
	$S_{3/2,\,1/2}$	$2/9$
	$S_{3/2,\,3/2}$	$5/18$
D_2 Absorption ($2\,^2S_{1/2} \rightarrow 2\,^2P_{3/2}$)	$S_{1/2\,,\,1/2}$	$2/9$
	$S_{1/2\,,\,3/2}$	$5/18$
	$S_{1/2\,,\,5/2}$	0
	$S_{3/2,\,1/2}$	$1/72$
	$S_{3/2,\,3/2}$	$1/9$
	$S_{3/2,\,5/2}$	$3/8$
D_2 Emission ($2\,^2P_{3/2} \rightarrow 2\,^2S_{1/2}$)	$S_{1/2\,,\,1/2}$	$2/9$
	$S_{1/2\,,\,3/2}$	$1/36$
	$S_{3/2,\,1/2}$	$5/36$
	$S_{3/2,\,3/2}$	$1/9$
	$S_{5/2,\,1/2}$	0
	$S_{5/2,\,3/2}$	$1/4$

Table 14: Relative Transition Strengths, $S_{F,\,F'}$, for ^{6}Li. Results are given in units of $\left|\left\langle J' \,\middle\|\, \hat{\mu}(1) \,\middle\|\, J \right\rangle\right|^2$.

the (+)-terms and σ^- for the (−)-terms) the atom must shuttle back and forth between these two states. No other internal states are possible. These transitions are known as the *photon-burst*, *cycling*, or *closed* transitions [20].

This behavior has a number of important implications. An atom interacting with near-resonant light on a photon-burst transition acts as a perfect two-level system—dramatically simplifying the theoretical treatment of the light-matter interaction. Further, the fact that the atom continually interacts with the light field significantly increases the magnitude of any interaction effect. There are two important instances of this behavior. First, the atomic cooling technique known as *optical molasses* uses repeated absorption-emission cycles to rapidly decelerate (and hence cool) atoms. For this reason, the photon-burst transition is also sometimes known as the *cooling* transition. Second, the photon-burst transition is maximally efficient at converting an incident probe beam into fluorescence—making this transition optimal for optical detection.

Because of the importance of the photon-burst transition, it is sometimes used as the unit of transition strength. To allow easy conversion to this viewpoint, the fundamental reduced matrix elements in Table 10 are also given in units of μ_0, the transition strength of the photon-burst transition.

7.4 Optical Rabi Frequency and Saturation Intensity

For a two-level atom coupled to a near-resonant optical field, we can compute the frequency at which the interaction coherently drives the atom between the two states. This frequency, known as the *optical Rabi frequency*, is given by [20]

$$\begin{aligned} \Omega &= \frac{\langle b \mid \hat{\boldsymbol{\mu}} \cdot \boldsymbol{E} \mid a \rangle}{h} \\ &= \frac{\mu_{ba} E_0}{h} \end{aligned} \tag{30}$$

where μ_{ba} is the electric-dipole transition matrix element for states a and b, and E_0 is the electric field strength of the incident optical field. We can write this in terms of laboratory units as

$$\Omega = 4.37\ \mu_{ba}\ \sqrt{I} \tag{31}$$

with Ω in MHz, μ in Debye, and I, the light intensity, in mW/mm^2.

When the Rabi frequency is less than the spontaneous decay rate Γ, (Tables 4 and 5), the atom is likely to spontaneously decay out of the excited state, rather than being driven coherently by the applied field. As the intensity of the applied field (and hence the electric field strength) increases, the Rabi frequency begins to dominate the spontaneous decay rate, and the atom-light interaction becomes stronger and more coherent. In the limit where the $\Omega \gg \Gamma$, the atom is being driven completely coherently, the atomic population is evenly split between the ground and excited levels, and increasing the light intensity ceases to affect the state populations. At this point, the transition is said to be *saturated*.

If we take the intensity of a light field to be $I = (1/2)c\epsilon_0 E^2$, we can define a *saturation intensity*, I_{sat}, given by

$$I_{sat} = \frac{c\epsilon_0 \Gamma^2 \hbar^2}{4\left|\boldsymbol{\mu} \cdot \boldsymbol{e}\right|^2}. \tag{32}$$

Property	Symbol	Value	Ref.
Representative D_1 Saturation Intensity	I_{sat} (D_1)	$7.59\,\mathrm{mW/cm^2}$	
Representative D_2 Saturation Intensity	I_{sat} (D_2)	$2.54\,\mathrm{mW/cm^2}$	

Table 15: Representative values of I_{sat} for the D_1 and D_2 lines of ^{6}Li.

In the above, $\boldsymbol{e}$ is the unit polarization vector of the light field such that $\boldsymbol{E} = E_0\boldsymbol{e}$. With this definition we find

$$\frac{I}{I_{sat}} = 2\left(\frac{\Omega}{\Gamma}\right)^2. \tag{33}$$

Hence, we can say a transition is saturated if $I \gg I_{sat}$. The factor of two is conventional, and being of order unity, does not materially affect whether a transition is saturated or not.

Note that the saturation intensity in (32) is transition-dependent. In a given line (D_1 or D_2) it is customary to report the smallest saturation intensity as a representative value. These values are tabulated in Table 15. The value for the D_2 line is particularly relevant, as it corresponds to the photon-burst transition.

8 Collisional Properties

The collisional properties of atoms play an important role in many cooling and trapping experiments. Sometimes this role is a negative one—for example, inelastic collisions between atoms change the internal state of the atoms, releasing large amounts of energy and perhaps ejecting one or more atoms from the trap. Other times collisions are harnessed and used by experimenters, such as in evaporative cooling, where elastic collisions eject hot atoms from the trap and rethermalize the remaining gas at a lower temperature.

The following sections are intended to provide an overview of the collisional properties of atoms in general and of ^{6}Li in particular. A much more thorough discussion of atomic collisions in general can be found in a number of standard texts such as [24–26]. A very detailed discussion of the collisional properties of ultracold ^{6}Li in particular can found in an earlier thesis from this research group [4].

8.1 The Scattering Problem

In an ultracold atomic gas, each atom is localized to a volume on the order of the cube of the deBroglie wavelength

$$\lambda_{dB} = \sqrt{\frac{2\pi\hbar^2}{mk_bT}}, \tag{34}$$

where m is the atomic mass, k_b is the Boltzmann constant, and T is the temperature of the gas. For ^{6}Li at a temperature of $1\,\mu$K we compute a deBroglie wavelength of $0.712\,\mu$m, which yields a localization volume of $3.61\times10^{-1}\,\mu\mathrm{m}^3$.

We can estimate the number of atoms in a given λ^3 volume by computing $N = n\lambda^3$, where n is the atomic number density for the gas. For most cooling and trapping experiments, this ranges from $1 \times 10^8\,\mathrm{cm}^{-3}$ to $1 \times 10^{14}\,\mathrm{cm}^{-3}$ at the most. For the localization volume given above, and using a moderate number density ($1 \times 10^{11}\,\mathrm{cm}^{-3}$) we calculate that, on average, there is only one atom per $\simeq 3000$ localization volumes. This value is not atypical.

For experiments in this regime, clearly an approach based on *binary* collisions (involving only two atoms) is reasonable. In such an approach, we treat the two-atom collision as the scattering of a single particle (of reduced mass, μ) off of an interaction potential. For ^{6}Li-^{6}Li collisions, the interaction potential will be some linear combination of the molecular *singlet* and *triplet* interaction potentials (determining the proper linear combination will be addressed in a future section).

In the singlet potential, the two atoms approach with their unpaired electronic spins antiparallel ($\boldsymbol{S} = \boldsymbol{S}_1 + \boldsymbol{S}_2 = 0$). Considering the symmetry of this state, we see that the spin wavefunction of the electrons is antisymmetric, requiring the spatial wavefunction to be symmetric. In such a case, the electrons are not excluded from the region between the nuclei, and the electrostatic attraction between electrons and nuclei leads to a deep potential well. In the triplet case, the two spins approach in the parallel configuration ($\boldsymbol{S} = 1$). Here the spin wavefunction is symmetric, requiring an antisymmetric spatial wavefunction. As a result, the electrons spend very little time in the region between nuclei, and the interaction potential is correspondingly weak.

The singlet and triplet molecular potentials were recreated in [4] from the results of several experiments that measured the potential in different regions. The potentials are plotted in Figure 9. The vertical axis is in units of cm^{-1}, while the radial coordinate is given in Bohr. Note that the singlet potential is significantly deeper than the triplet, as expected.

While the binary collision approach is a useful starting point, it is of course incomplete. In experiments with degenerate or near degenerate gases, the number of atoms per localization region necessarily approaches or exceeds one (indeed, this is the very definition of degeneracy). In such cases, and in other extreme situations where the the atomic interactions are resonantly enhanced, three-body collisions do play an increasingly important role—often becoming the a limiting process. Such effects are beyond the scope of this chapter, but the reader is advised to keep their existence in mind.

Strictly speaking, once the interaction potential is known, we have only to solve the full Schrödinger equation

$$(\nabla^2 + k^2)\Psi_{\boldsymbol{k}} = \frac{2\mu}{\hbar^3}\, V\, \Psi_{\boldsymbol{k}} \tag{35}$$

for solutions of the form

$$\Psi_{\boldsymbol{k}} = e^{i\boldsymbol{k}\cdot\boldsymbol{r}} + \Psi_{scat}, \tag{36}$$

where the first term on the right is a plane wave representing the incoming particle, and the second term represents the outgoing scattered wavefunction. In fact, such an approach, while correct, misses an important simplification that we can make for the case ultracold gases.

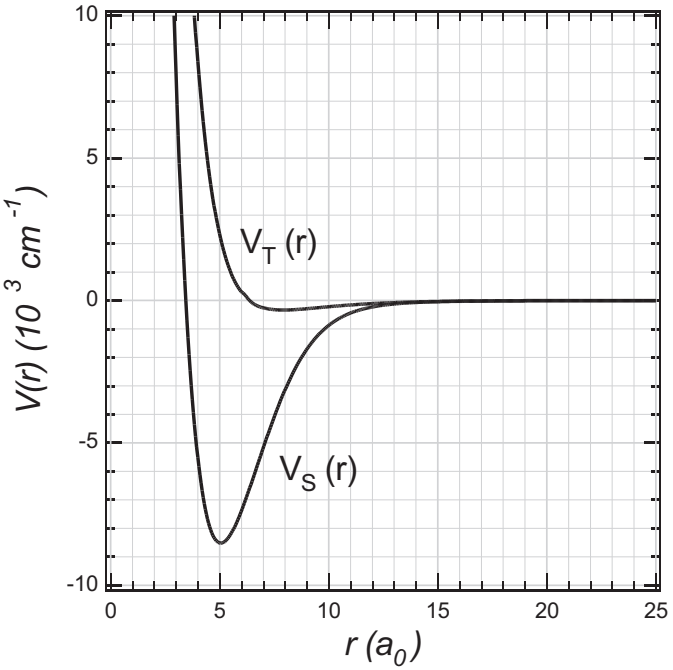

Figure 9: Singlet and Triplet Molecular Potentials of ^{6}Li.

8.2 Partial Wave Treatment—The Benefit of Ultracold Gases

When the interaction potential is a central potential (as it is in this case), there is no ϕ-dependence in our solution (taking the z-axis of the spherical coordinate system along the direction of propagation of the incoming particle). In this case, we can expand both the incoming and scattered wavefunctions in an angular momentum basis—the coefficients of this expansion are known as the *partial-wave amplitudes*. Since a central potential cannot change angular momentum, the single Schrödinger equation above becomes an infinite sum of Schródinger equations, *one for each angular momentum component*, which are solved separately. At first glance, this hardly seems an improvement, as we have apparently increased the complexity of the problem enormously. However, it is the case that at low temperatures, only a few of the the partial wave amplitudes are distinguishable from zero. A heuristic explanation of this is provided in [24], as well as almost any other scattering text.

In the case of an *ultracold* atomic gas, we can go even further. In general, only the lowest-order term, the *s-wave* term provides a contribution. This is the power of the partial wave approach as applied to ultracold gases—we again have a single Schrödinger equation, but in that we are working with a single angular momentum component, the analysis is greatly simplified. (At this point, the reader is cautioned that the "only s-wave" approach, much like the "binary collision" approach above, is only an approximation. It appears that in the case of ultracold gases with resonantly enhanced interactions, p-wave and higher interactions may play an important role in the interesting physics that arise.)

The primary physical parameter that we hope to compute with scattering theory is the *total cross section*, σ. The total cross section is dimensionally an area (length^2) and physically represents how large of a "target" the atom presents to other atoms. The rates

at which collisions occur in the gas are determined by the atomic number density, n, the gas temperature, T, and the collision cross-sections, σ.

In the partial wave expansion, the total cross section is a sum of partial cross sections, σ_L. For *indistinguishable* particles, the partial wave cross-section for a symmetric spatial state (even L) is given by

$$\sigma_L = \frac{8\pi}{k^2}(2L+1)\sin^2\delta_L. \tag{37}$$

In the above, k is the wavenumber for the incoming particle, and δ_L is the *partial wave phase shift*—the phase imposed on the partial wave by the existence of the potential. Note that since sin is bounded by 0 and 1, σ_L is necessarily positive, and has a maximum value of

$$\sigma_L^{max} = \frac{8\pi}{k^2}(2L+1). \tag{38}$$

This limit is known as the *unitarity* limit and occurs when δ_L is an odd multiple of $\pi/2$.

In the case where we have only s-wave scattering, the total cross section is the s-wave partial cross section

$$\sigma = \sigma_{L=0} = \frac{8\pi}{k^2}\sin^2\delta_{L=0}. \tag{39}$$

At this point, the problem of finding the total cross section has been reduced to finding the s-wave phase shift. While it is possible to compute the wavefunction both with and without the interaction potential, and compare the two to extract the phase shift, the next section delineates an approach that is both simpler and more elegant.

8.3 The S-Wave Scattering Length

In the low-energy limit ($k \to 0$), it is possible to show that for a large class of potentials, we can write $\tan\delta_0 \propto k$, and hence also $\sin\delta_0 \propto k$ [25]. We can then define the proportionality constant

$$a \equiv -\lim_{k\to 0}\frac{\sin\delta_0(k)}{k}. \tag{40}$$

This constant is known as the *s-wave scattering length*. When this result is inserted into (39), we get the low energy result

$$\sigma = 8\pi a^2. \tag{41}$$

It is important to note that by taking the low-energy limit, the scattering length depends only on the interaction potential and not on the incoming wavenumber (which we treat as zero). Thus we must only compute the scattering lengths for interactions of different pairs of internal ^{6}Li states, and then we have completely characterized the problem.

The scattering length has a simple geometric interpretation. The radial wavefunctions, in the asymptotic limit, have the low energy form $\sin(kr+\delta_0) \simeq \sin(kr)+\delta_0\cos(kr) \to k(r-a)$ as $k \to 0$. This limiting form is a straight line with x-intercept a. The scattering length can thus be computed by calculating the asymptotic wavefunction, and projecting backwards to find the x-intercept. The sign of the scattering length indicates the overall effect of the potential. A negative scattering length indicates a potential which is overall attractive, which a positive scattering length represents an overall repulsive potential. A schematic of the geometrical meaning of the scattering length is shown in Figure 10.

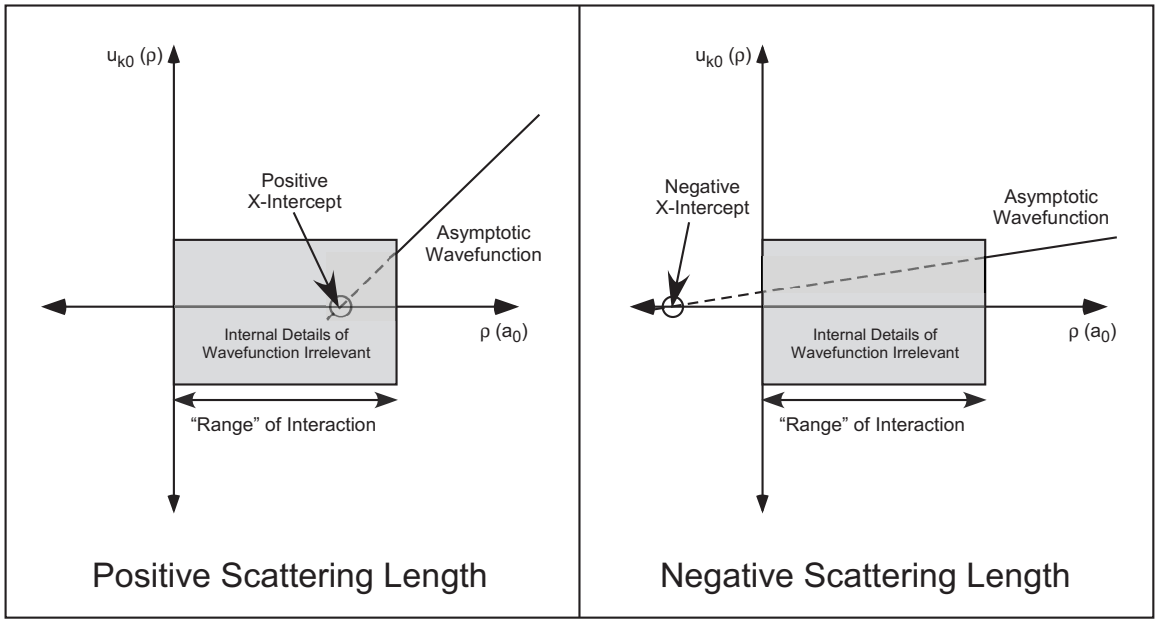

Figure 10: Determination of Scattering Length.

Property	Symbol	Value	Ref.
Singlet S-Wave Scattering Length	a_s	38.75 Bohr	[4, 27, 28]
Triplet S-Wave Scattering Length	a_t	-2240 Bohr	[4, 27, 28]

Table 16: Singlet and triplet s-wave scattering lengths of ^{6}Li.

8.3.1 Singlet and Triplet Scattering Length

In Section 8.1, it was mentioned that all ^{6}Li-^{6}Li interaction potentials could be described by a linear combination of the molecular singlet and triplet potentials. As we have seen in the preceding sections, for ultracold gases, the effect of an interaction potential can be characterized by a single parameter, the s-wave scattering length, a. The combination of these two facts means all ultracold ^{6}Li-^{6}Li interactions can be characterized by a linear combination of singlet and triplet s-wave scattering lengths. In [4], the values of these scattering lengths are computed from the most recent measurements of the molecular potentials, and the results are in good agreement with experiment [27, 28]. The values of the scattering lengths are given in Table 16.

It is worth noting the enormously large and negative triplet scattering length. An admixture of states that admits even a small amount of the triplet state will have a scattering length with is both large and negative. These properties are very desirable for studies of ultracold fermions. This scattering length is the largest in any alkali system, and is why ^{6}Li is so appealing to researchers in the field.

The large triplet scattering length arises from a *zero energy resonance* in the triplet molecular potential. As we have seen, for ultracold gases, the incoming kinetic energy is zero

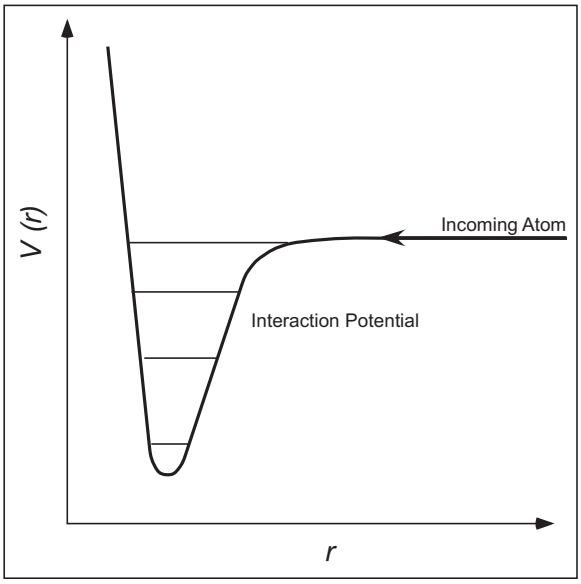

Figure 11: Phenomenology of a zero-energy resonance.

to a good approximation. It turns out that the molecular triplet potential has a quasi-bound state lying just above zero. That is, if the triplet potential were even 0.03% deeper, it would be able to support another bound state. On a heuristic level, this quasi-bound state is able to "capture" an incoming particle for a short period of time prior to allowing it to scatter outward. This dramatically increases the effect of the potential, and hence the size of the scattering length. This state of affairs is depicted in Figure 11.

Mathematically, we can see how this arises by considering (37). It can be shown that when a potential is at a depth such that a state is transferring from bound to unbound, the partial wave phase shift is exactly $\pi/2$. Hence the partial wave cross section in (37) becomes

$$\sigma_L = \frac{8\pi}{k^2}, \tag{42}$$

which diverges in the low-energy ($k \to 0$) limit.

8.3.2 Wavefunction Symmetry and the $|1\rangle$-$|2\rangle$ Mixture

We begin by considering the symmetry of the wavefunction for an ultracold ^{6}Li-^{6}Li collision. The two-particle wavefunction is a product of three terms: the center-of-mass wavefunction (describing where in the trap the collision takes place), the spatial wavefunction (describing the relative position of the atoms), and the spin wavefunction (describing the intrinsic angular momenta of the atoms). Since ^{6}Li is a composite fermion, the overall wavefunction must be antisymmetric. The center-of-mass wavefunction is clearly symmetric, as switching the two indistinguishable particles has no effect on that term. As a result, the product of the spatial and spin wavefunctions must be antisymmetric.

Now as we have seen before, ultracold collisions are dominated by s-wave interactions. However, s-wave interactions require symmetric spatial wavefunctions. Hence, they also imply antisymmetric spin wavefunctions. This fact underlies one of the most important

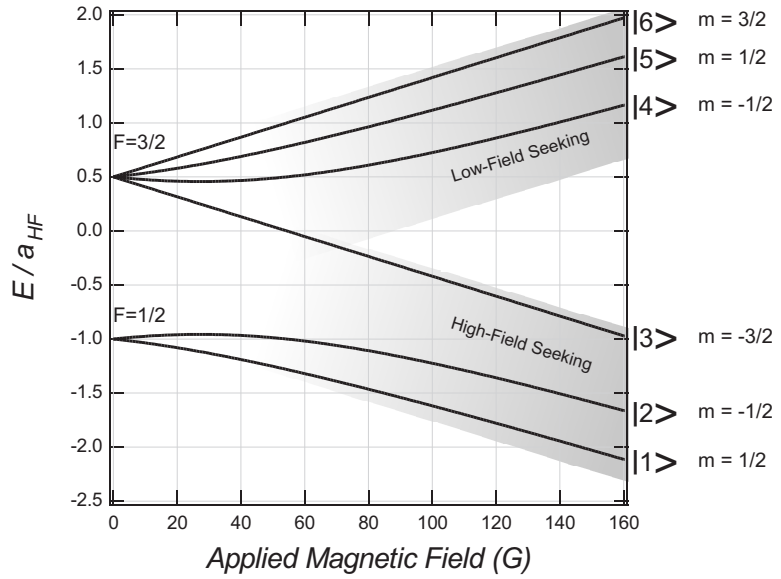

Figure 12: Ground state hyperfine structure of ^{6}Li. The states are numbered $|1\rangle$-$|6\rangle$ in order of increasing energy in a magnetic field. The vertical axis is plotted in units of the magnetic-dipole hyperfine constant for the ground state.

features of ultracold fermionic gases: *spin-polarized mixtures are non-interacting*. A single spin state cannot exist in an antisymmetric spin state. Hence, the spatial wavefunction must be antisymmetric. But antisymmetric spatial wavefunctions can only interact via p-wave (and higher odd) interactions—which are highly suppressed at ultracold temperatures.

Thus, groups wishing to study an interacting fermi gas of ^{6}Li must work with a *mixture* of two or more spin states. But which ones? Consider the states shown in Figure 12, which shows the magnetic-field dependence of the hyperfine ground states. The states are numbered with what has become standard nomenclature in ^{6}Li; $|1\rangle$-$|6\rangle$, in order of increasing energy in a magnetic field. Further, each state is listed with its z-component of angular momentum. This is useful, as s-wave collisions conserve the total magnetic quantum number.

For the current and future experiments, our group has chosen to work with a mixture of states $|1\rangle$ and $|2\rangle$. This mixture has a number of important properties. First, it has the lowest internal energy of any interacting mixture (a sample purely in the $|1\rangle$ state would not be interacting for reasons stated above). The low-energy nature of the mixture is important because many higher-energy mixtures have open inelastic collision channels whereby an atom can change internal state and release enough energy to eject one or more atoms from the trap. Mixtures with open inelastic channels tend to destroy themselves. Second, at zero-field, the $|1\rangle$-$|2\rangle$ mixture consists of states that are in some sense mirror images of one another—they differ only in the sign of their magnetic quantum number. This makes the mixture particularly well-suited for future studies of superfluidity. Third, the states in the mixture are *high-field seeking*—that is, when placed in a magnetic gradient, they are drawn to regions of high field. Such states cannot be trapped in a magnetic trap (magnetic traps can produce local minima in the magnetic field strength, but local maxima are forbidden). Since we trap and directly cool in an optical trap, this has no effect on us. Other groups wishing to study

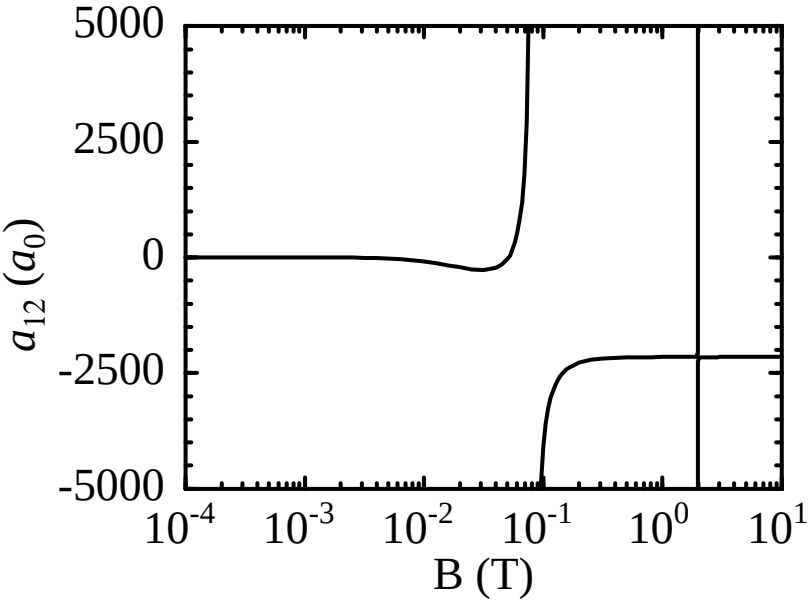

Figure 13: S-wave scattering length For $|1\rangle$-$|2\rangle$ collisions. The vertical axis is in units of Bohr.

this mixture, however, must magnetically trap and cool another ^{6}Li mixture, then transfer that mixture to an optical trap, and then finally convert the atoms to a $|1\rangle$-$|2\rangle$ mixture in some manner. We believe the relative complexity of these steps gives us a competitive advantage. There are two, additional, *serendipitous* features of the $|1\rangle$-$|2\rangle$ mixture that will be discussed below.

Having decided on the $|1\rangle$-$|2\rangle$ mixture, we must determine its collisional properties. In fact, this has been done in [15], via a complete coupled-channel calculation. The result of their calculation, a plot of the s-wave scattering length as a function of applied magnetic field is shown in Figure 13. There are three items of particular importance in this graph. First, the scattering length appears to be exactly zero at zero applied field. This is not an artifact of the scale of the plot. The authors claim the value was always zero to within the precision of their calculation. There is no obvious symmetry argument for why this value should be zero. We, and the authors, believe it to be an accidental feature of the $|1\rangle$-$|2\rangle$ mixture. The other two notable items are the resonances at $\simeq$850 G and $\simeq$1.3 T. These resonances, known as *Feshbach resonances* [29], result when the incoming particle has the same energy as a bound state in an energetically closed collision channel. For example, the $|1\rangle$-$|2\rangle$ mixture, on solely angular momentum grounds, can convert to $|3\rangle$-$|6\rangle$ or $|4\rangle$-$|5\rangle$ (all have total m=0). However, the internal energy of the $|1\rangle$-$|2\rangle$ mixture is such that, for temperatures less than $\simeq$10 mK, these channels are not energetically allowed. But molecular bound states in these channels exist, and for certain magnetic fields, the bound states are resonant with the incoming particles. A schematic of this process is shown in Figure 14. The practical result is to allow magnetic tuning of the scattering length in both magnitude and sign.

These three points of note in the scattering length are the serendipitous features of the

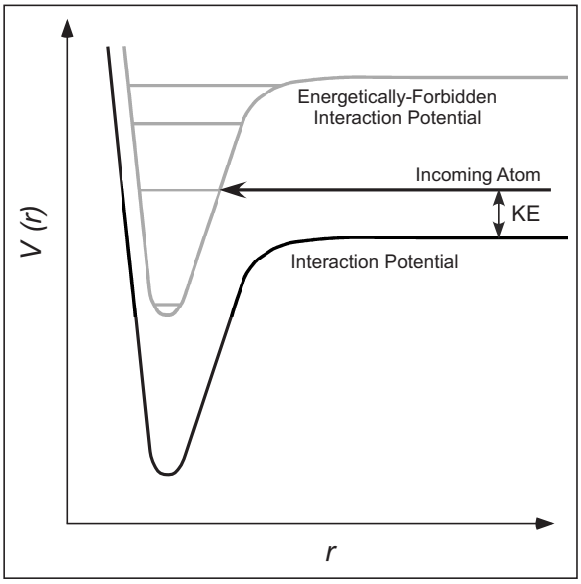

Figure 14: Phenomenology of a Feshbach Resonance.

$|1\rangle$-$|2\rangle$ mixture mentioned above. The fact that the scattering length is zero at zero applied field means that *the* $|1\rangle$-$|2\rangle$ *mixture can be switched from interacting to noninteracting by simply turning off the applied field*. Further, the existence of a Feshbach resonance means that not only can we explore strongly- and weakly-interacting mixtures (by magnetically-tuning the magnitude of the scattering length), but that we can also change the sign of of the interactions, switching from attractive to repulsive, or vice-versa. Thus we have complete control of not only whether the mixture is interacting or noninteracting, but also over the type and strength of the interaction. Much of the exciting physics of fermionic gases depends on the details of the interatomic interaction—working with this mixture means we have the capability to easily explore all the possible regimes.

References

[1] M. E. Gehm. *Preparation of an Optically-Trapped Degenerate Fermi Gas of* ^{6}*Li: Finding the Route to Degeneracy*. PhD thesis, Duke University, 2003.

[2] D. A. Steck. Cesium D line data.
see `http://george.ph.utexas.edu/~dsteck/alkalidata`., 2000.

[3] D. A. Steck. Sodium D line data.
see `http://george.ph.utexas.edu/~dsteck/alkalidata`., 2000.

[4] K. M. O'Hara. *Optical Trapping and Evaporative Cooling of Fermionic Atoms*. PhD thesis, Duke University, 2000.

[5] R. C. Weast, M. J. Astle, and W. H. Beyer, editors. *CRC Handbook of Chemistry and Physics*. CRC Press, Boca Raton, 64th edition, 1983.

[6] A. N. Nesmeyanov. *Vapour Pressure of the Elements*. Academic Press, New York, 1963.

[7] I. Mills, T. Cvitas, K. Homann, N. Kallay, and K. Kuchitsu. *Quantities, Units, and Symbols in Physical Chemsitry*. Blackwell Scientific Publishing, Oxford, 1988.

[8] W. I. McAlexander, E. R. I. Abraham, and R. G. Hulet. Radiative lifetime of the $2P$ state of lithium. *Phys. Rev. A*, 54(1):R5, July 1996.

[9] Roger C. Brown, Saijun Wu, J. V. Porto, Craig J. Sansonetti, C. E. Simien, Samuel M. Brewer, Joseph N. Tan, and J. D. Gillaspy. Quantum interference and light polarization effects in unresolvable atomic lines: Application to a precise measurement of the ^{6,7}li D_2 lines. *Phys. Rev. A*, 87:032504, Mar 2013.

[10] R. Liboff. *Introductory Quantum Mechanics*. Addison-Wesley, New York, 2nd edition, 1993.

[11] P. J. Mohr and B. N. Taylor. CODATA recommended values of the fundamental physical constants: 1998. *Rav. Mod. Phys.*, 72, 2000.

[12] I. I. Sobel'man. *Introduction to the Theory of Atomic Spectra*. Pergamon Press, Oxford, 1972.

[13] E. Arimondo, M. Inguscio, and P. Violino. Experimental determinations of the hyperfine structure in the alkali atoms. *Rev. Mod. Phys.*, 49(1):31, January 1977.

[14] J. Walls, R. Ashby, J. Clarke, B. Lu, and W. Wijngaarden. Measurement of isotope shifts, fine and hyperfine structure splittings of the lithium D lines. preprint provided in private communication, 2002.

[15] M. Houbiers, H. T. C. Stoof, W. I. McAlexander, and R. G. Hulet. Elastic and inelastic collisions of ^{6}Li atoms in magnetic and optical traps. *Phys. Rev. A*, 57(3):R1497, March 1998.

[16] R. W. Schmieder, A. Lurio, and W. Happer. Quadratic Stark effect in the $^2P_{3/2}$ states of the alkali atoms. *Phys. Rev. A*, 3(4):1209, April 1971.

[17] A Khadjavi, A. Lurio, and W. Happer. Stark effect in excited states of Rb, Cs, Cd, and Hg. *Phys. Rev.*, 167(1):128, March 1968.

[18] R. W. Molof, H. L. Schwartz, T. M. Miller, and B. Bederson. Measurments of electric dipole polarizabilities of the alkali-metal atoms and the metastable noble gas atoms. *Phys. Rev. A*, 10(4):1131, October 1974.

[19] L. Windholz, M. Musso, G Aerza, and H. Jäger. Precise Stark-effect investigations of the lithium D_1 and D_2 lines. *Phys. Rev. A*, 46(9):5812, November 1992.

[20] Leslie Allen and Joseph H. Eberly. *Optical Resonance and Two-Level Atoms*. Dover Publications, 1975.

[21] A. R. Edmonds. *Angular Momentum in Quantum Mechanics*. Princeton University Press, 1960.

[22] J. E. Thomas. Lecture Notes—Quantum Mechanics I.
Lecture notes from a course taught at Duke University, 1995.

[23] Rodney Loudon. *The Quantum Theory of Light*. Clarendon Press, Oxford, 1983.

[24] E. Merzbacher. *Quantum Mechanics*. John Wiley and Sons, New York, 3rd edition, 1998.

[25] C. J. Joachain. *Quantum Collision Theory*. North-Holland Publishing Company, 1983.

[26] N. F. Mott and H. S. W. Massey. *The Theory of Atomic Collisions*. Clarendon Press, Oxford, 1965.

[27] E. R. I. Abraham, W. I. McAlexander, J. M. Gerton, R. G. Hulet, R. Côté, and A. Dalgarno. Triplet s-wave resonance in ^{6}Li collisions and scattering lengths of ^{6}Li and ^{7}Li. *Phys. Rev. A*, 55(5):R3299, May 1997.

[28] K. M. O'Hara, M. E. Gehm, S. R. Granade, S. Bali, and J. E. Thomas. Stable, strongly attractive, two-state mixture of lithium fermions in an optical trap. *Phys. Rev. Lett.*, 85(10):2092, September 2000.

[29] Herman Feshbach. A unified theory of nuclear reactions. II. *Ann. Phys.*, 19:287, 1962.